

## Hydrogen Storage

## A Composite of Complex and Chemical Hydrides Yields the First Al-Based Amidoborane with Improved Hydrogen Storage Properties

Iurii Dovgaliuk,<sup>[a]</sup> Lars H. Jepsen,<sup>[b]</sup> Damir A. Safin,<sup>[a]</sup> Zbigniew Łodziana,<sup>[c]</sup> Vadim Dyadkin,<sup>[d]</sup> Torben R. Jensen,<sup>[b]</sup> Michel Devillers,<sup>[a]</sup> and Yaroslav Filinchuk<sup>\*[a]</sup>

**Abstract:** The first Al-based amidoborane Na[Al(NH<sub>2</sub>BH<sub>3</sub>)<sub>4</sub>] was obtained through a mechanochemical treatment of the NaAlH<sub>4</sub>-4 AB (AB = NH<sub>3</sub>BH<sub>3</sub>) composite releasing 4.5 wt% of pure hydrogen. The same amidoborane was also produced upon heating the composite at 70 °C. The crystal structure of Na[Al(NH<sub>2</sub>BH<sub>3</sub>)<sub>4</sub>], elucidated from synchrotron X-ray powder diffraction and confirmed by DFT calculations, contains the previously unknown tetrahedral ion [Al(NH<sub>2</sub>BH<sub>3</sub>)<sub>4</sub>]<sup>-</sup>, with every NH<sub>2</sub>BH<sub>3</sub><sup>-</sup> ligand coordinated to aluminum through nitrogen atoms. Combination of complex and chemical hydrides in the same compound was possible due to both the lower stability of the Al-H bonds compared to the B-H ones in borohydride, and due to the strong Lewis acidity of Al<sup>3+</sup>. According to the thermogravimetric analysis-differential scanning calorimetry-mass spectrometry (TGA-DSC-MS) studies, Na[Al(NH<sub>2</sub>BH<sub>3</sub>)<sub>4</sub>] releases in two steps

9 wt% of pure hydrogen. As a result of this decomposition, which was also supported by volumetric studies, the formation of NaBH<sub>4</sub> and amorphous product(s) of the surmised composition AlN<sub>4</sub>B<sub>3</sub>H<sub>(0-3.6)</sub> were observed. Furthermore, volumetric experiments have also shown that the final residue can reversibly absorb about 27% of the released hydrogen at 250 °C and *p*(H<sub>2</sub>) = 150 bar. Hydrogen re-absorption does not regenerate neither Na[Al(NH<sub>2</sub>BH<sub>3</sub>)<sub>4</sub>] nor starting materials, NaAlH<sub>4</sub> and AB, but rather occurs within amorphous product(s). Detailed studies of the latter one(s) can open an avenue for a new family of reversible hydrogen storage materials. Finally, the NaAlH<sub>4</sub>-4 AB composite might become a starting point towards a new series of aluminum-based tetraamidoboranes with improved hydrogen storage properties such as hydrogen storage density, hydrogen purity, and reversibility.

## Introduction

Current concerns over environmental pollution are pushing the development of carbon-neutral energy carriers. Among these carriers, hydrogen has emerged as an ideal candidate. However, there are numerous challenges in its practical application. In order for hydrogen to be used as an environmentally

benign energy carrier, efficient storage methods must be developed. This has been a main challenge during the last decades with much research focused on the increasing amount of hydrogen stored per given mass of a support. Recently, the U.S. Department of Energy introduced ultimate targets of 7.5 wt% and 70 g L<sup>-1</sup> for the gravimetric and volumetric capacities of hydrogen, respectively.<sup>[1]</sup> These and other technical limitations have reduced the number of potential hydrogen storage systems, giving an advantage to complex metal hydrides with high hydrogen content.<sup>[2,3]</sup>

Alkali-metal alanates, M(AlH<sub>4</sub>)<sub>*n*</sub>, have shown remarkable hydrogen storage properties. For example, NaAlH<sub>4</sub>, the most intensively studied member of this class of compounds, has a reversible hydrogen capacity of 5.6 wt%.<sup>[4]</sup> However, high de- and rehydrogenation temperatures for alanates (e.g., 210–220 °C for NaAlH<sub>4</sub>) as well as a moderate hydrogen content have directed attention to lighter complex hydrides such as borohydrides, M(BH<sub>4</sub>)<sub>*n*</sub>.<sup>[2,3]</sup> At the same time, reversible systems based on borohydrides were developed only in the form of reactive hydride composites (RHCs), containing complex and binary metal hydrides. In particular, the reversible system, comprising LiBH<sub>4</sub> and MgH<sub>2</sub>, doped with TiCl<sub>3</sub> to catalyze rehydrogenation, yields 8–10 wt% of hydrogen according to the following reaction [Eq. (1)].<sup>[5,6]</sup>

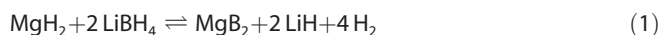
[a] I. Dovgaliuk, Dr. D. A. Safin, Prof. M. Devillers, Prof. Y. Filinchuk  
Institute of Condensed Matter and Nanosciences  
Université catholique de Louvain, Place L. Pasteur 1  
1348 Louvain-la-Neuve (Belgium)  
E-mail: yaroslav.filinchuk@uclouvain.be

[b] L. H. Jepsen, Prof. T. R. Jensen  
Center for Materials Crystallography  
Interdisciplinary Nanoscience Center and  
Department of Chemistry, Aarhus University  
Langelandsgade 140, 8000 Aarhus C (Denmark)

[c] Prof. Z. Łodziana  
Department of Structural Research, INP Polish Academy of Sciences  
ul. Radzikowskiego 152, 31–342 Kraków (Poland)

[d] Dr. V. Dyadkin  
Swiss-Norwegian Beam Lines  
European Synchrotron Radiation Facility  
Rue Horowitz 6, 38043 Grenoble (France)

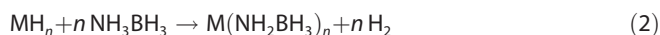
Supporting information for this article is available on the WWW under <http://dx.doi.org/10.1002/chem.201501302>.



In the middle of the last decade, an intensive research has been focused on the so-called chemical hydrides, in particular ammonia borane (AB),  $\text{NH}_3\text{BH}_3$ .<sup>[7,8]</sup> The high hydrogen content in AB (about 19.6 wt%,  $152\text{ g L}^{-1}$ ) and its stability under ambient conditions have attracted significant attention to this compound.<sup>[9]</sup> Ammonia borane undergoes stepwise decomposition with 6.5 wt% of hydrogen released below  $112^\circ\text{C}$  and the total amount of 14.5 wt% at about  $200^\circ\text{C}$ . However, this release is accompanied by the evolution of undesirable borazine,  $(\text{BHNH})_3$ , aminoborane,  $\text{BH}_2\text{NH}_2$ , and diborane,  $\text{B}_2\text{H}_6$ .<sup>[10,11]</sup> Another disadvantage of practical applications of AB as a hydrogen storage material arises from its spectacular foaming leading to dramatic volume expansion during its thermolysis.

A significant improvement in the hydrogen release temperature was achieved by forming metal amidoboranes (MABs),  $\text{M}(\text{NH}_2\text{BH}_3)_n$ , from AB and metal hydrides, thereby decreasing the decomposition temperature to about  $90^\circ\text{C}$  for  $\text{M}=\text{Li}^+$  and  $\text{Na}^+$ .<sup>[12]</sup> Recently, numerous MABs ( $\text{M}=\text{Li}^+$ ,  $\text{Na}^+$ ,  $\text{K}^+$ ,  $\text{Mg}^{2+}$ ,  $\text{Ca}^{2+}$ ,  $\text{Sr}^{2+}$ ,  $\text{Y}^{3+}$ ),<sup>[12–18]</sup> including the mixed-metal compounds  $\text{Na}[\text{Li}(\text{NH}_2\text{BH}_3)_2]$ ,<sup>[19]</sup>  $\text{Na}_2[\text{Mg}(\text{NH}_2\text{BH}_3)_4]$ ,<sup>[20]</sup> and  $\text{K}_2[\text{Mg}(\text{NH}_2\text{BH}_3)_4]$ ,<sup>[21]</sup> have been obtained and characterized. Although all the listed MABs release  $\text{NH}_3$  and  $\text{NH}_2\text{BH}_2$  in addition to hydrogen,  $\text{LiNH}_2\text{BH}_3 \cdot \text{NH}_3\text{BH}_3$  produces up to 14.0 wt% of pure hydrogen upon heating to  $230^\circ\text{C}$ .<sup>[22]</sup> A system that can reversibly release pure hydrogen at lower temperatures is seen as the ultimate goal for practical hydrogen storage.

The formation of metal amidoboranes starting from binary hydrides and AB can be considered by itself as a method to produce hydrogen. In this case, the  $\text{MH}_n\text{-AB}$  ( $\text{M}=\text{Li}^+$ ,  $\text{Na}^+$ ,  $\text{K}^+$ ,  $\text{Ca}^{2+}$ ,  $\text{Mg}^{2+}$ ,  $\text{Al}^{3+}$ ,  $\text{Y}^{3+}$ )<sup>[18,23,24]</sup> mixtures can be considered as RHCs according to the following reaction [Eq. (2)]:



Although this reaction releases hydrogen under mild conditions (e.g.,  $\approx 70^\circ\text{C}$  for  $\text{M}=\text{Mg}^{2+}$ ),<sup>[16]</sup> it is of low purity,  $\sim 90\%$  for  $\text{M}=\text{Li}^+$ ,  $\text{Mg}^{2+}$ , and  $\text{Al}^{3+}$ , and can also be contaminated by a large amount of  $\text{NH}_3$  as it was observed for  $\text{M}=\text{Na}^+$  and  $\text{Ca}^{2+}$ .<sup>[23]</sup>

By contrast, the lithium- or sodium-containing composites of alanates with AB release relatively pure hydrogen.<sup>[23,25,26]</sup> The alanates are not binary, like in the reaction given in Equation (2), but complex hydrides; and the reaction pathways for these Al-based systems are not yet determined. Thus, understanding the behavior of the Al-based composites can help to develop a new family of materials with improved hydrogen storage properties. This goal prompted current studies of the composition, structure, and reaction mechanisms of the hydrogen release in the alanate–AB systems. By combining the beneficial properties of the hydrogen storage systems based on aluminum, boron, and nitrogen, new possibilities to create a reversible high hydrogen density storage material are generated.

This work is focused on the  $\text{NaAlH}_4\text{-4AB}$  system, where the first Al-based amidoborane,  $\text{Na}[\text{Al}(\text{NH}_2\text{BH}_3)_4]$ , is obtained. Crystallographic studies allowed determining its composition and

structure, thus, defining the previously unexplored, but favorable 1:4 stoichiometry of the starting composite.  $\text{Na}[\text{Al}(\text{NH}_2\text{BH}_3)_4]$  forms through either mechanochemical treatment at room temperature or by heating the mixture up to approximately  $70^\circ\text{C}$  according to the following Equation (3):



It was found that the reaction given in Equation (3) is slightly exothermic and non-reversible. However,  $\text{Na}[\text{Al}(\text{NH}_2\text{BH}_3)_4]$  also releases, in two steps, additionally up to eight equivalents of  $\text{H}_2$ . Remarkably, this desorption is partially reversible. Thus, the decomposition properties of  $\text{Na}[\text{Al}(\text{NH}_2\text{BH}_3)_4]$  were systematically investigated by in situ synchrotron radiation X-ray powder diffraction (SRXRPD), by thermal analysis coupled with mass spectrometry, by temperature-programmed photographic analysis, and by volumetric methods. It was established that the hydrogen re-absorption does not regenerate  $\text{NaAlH}_4$  or  $\text{Na}[\text{Al}(\text{NH}_2\text{BH}_3)_4]$ , but rather occurs between the amorphous product(s) and intermediate(s) of the dehydrogenation process.

$\text{Na}[\text{Al}(\text{NH}_2\text{BH}_3)_4]$  is the first compound coming from the combination of a complex and chemical hydrides, its formation is favored by the lower stability of the Al–H bonds compared to the B–H ones, and due to the Lewis acidity of the complex-forming aluminum cation. Furthermore, the  $\text{NaAlH}_4\text{-4AB}$  system opens a route to design a series of aluminum tetraamidoboranes by using, for example, other alkali and alkali-earth metal alanates instead of  $\text{NaAlH}_4$ , with improved hydrogen storage properties.

## Results and Discussion

### Phase analysis and in situ SRXRPD data

The in situ SRXRPD patterns have been collected from room temperature to  $150^\circ\text{C}$  ( $5^\circ\text{C min}^{-1}$ ) (Figure 1) for the  $\text{NaAlH}_4\text{-4AB}$  mixture **s1**, obtained after 160 milling/break cycles (Table 1). The temperature-dependent composition of **s1**, extracted from the sequential Rietveld refinement, is given in Figure 1.

At room temperature **s1** contains Bragg reflections from  $\text{AB}$ <sup>[27]</sup> (26.3 wt%),  $\text{NaAlH}_4$ <sup>[28]</sup> (18.5 wt%), and from the previously unknown  $\text{Na}[\text{Al}(\text{NH}_2\text{BH}_3)_4]$  (55 wt%). Peaks from AB disappear at around  $90^\circ\text{C}$  without the appearance of new peaks. At the same time, the intensities of the peaks of  $\text{Na}[\text{Al}(\text{NH}_2\text{BH}_3)_4]$  are continuously increasing and the peaks become narrower. According to the sequential refinement, the weight fraction of  $\text{Na}[\text{Al}(\text{NH}_2\text{BH}_3)_4]$  increases after approximately  $80^\circ\text{C}$ , due to the reaction of AB with  $\text{NaAlH}_4$  (Figure 1). Its peaks disappear at about  $120^\circ\text{C}$  with an appearance of peaks for  $\text{NaBH}_4$  implying also the formation of amorphous product(s).

Complementary measurements on the  $\text{NaAlH}_4\text{-4AB}$  mixture **s2** (Table 1), obtained after twenty milling/break cycles, exhibited the formation of a negligible amount of  $\text{Na}[\text{Al}(\text{NH}_2\text{BH}_3)_4]$  (Figure S1 in the Supporting Information). Thus, mixture **s2**, being a homogenous physical mixture of AB and  $\text{NaAlH}_4$ , was

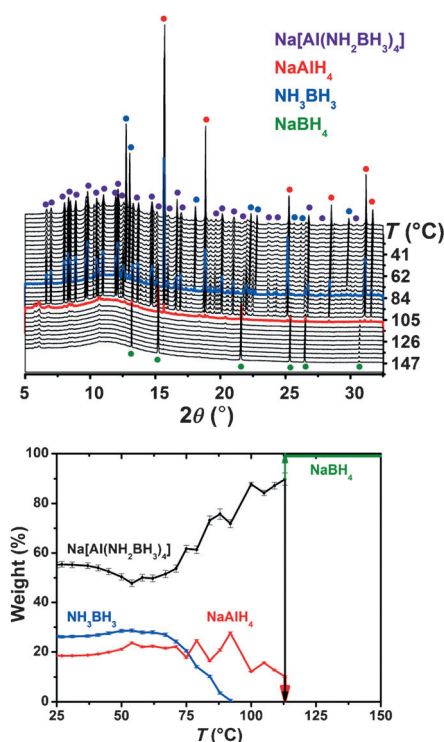


**Figure 1.** Top) Variable-temperature plot of the SRXRPD patterns of **s1** (SNBL/ESRF synchrotron,  $\lambda = 0.823065 \text{ \AA}$ ), and bottom) fractional content of compounds extracted from the Rietveld refinement of the powder patterns.

Table 1. Samples studied in this work.		
Sample	Synthetic approach	Phase composition from XRPD [wt %]
<b>s1</b>	NaAlH <sub>4</sub> -4 AB 160 milling/break cycles of 3/5 min	≈ 55 of Na[Al(NH <sub>2</sub> BH <sub>3</sub> ) <sub>4</sub> ] ≈ 26 of NH <sub>3</sub> BH <sub>3</sub> ≈ 19 of NaAlH <sub>4</sub>
<b>s2</b>	NaAlH <sub>4</sub> -4 AB 20 milling/break cycles of 3/3 min	≈ 83 of NH <sub>3</sub> BH <sub>3</sub> ≈ 17 of NaAlH <sub>4</sub>
<b>s3</b>	NaAlH <sub>4</sub> -4 AB 240 milling/break cycles of 3/5 min	≈ 90 of Na[Al(NH <sub>2</sub> BH <sub>3</sub> ) <sub>4</sub> ] ≈ 4 of NH <sub>3</sub> BH <sub>3</sub> ≈ 6 of NaAlH <sub>4</sub>
<b>s4</b>	NaAlH <sub>4</sub> -4 AB doped with 2 mol % of TiCl <sub>3</sub> 240 milling/break cycles of 3/5 min	≈ 88 of Na[Al(NH <sub>2</sub> BH <sub>3</sub> ) <sub>4</sub> ] ≈ 11 of NH <sub>3</sub> BH <sub>3</sub> ≈ 1 of NaAlH <sub>4</sub>

used to examine the temperature as a stimulus of the formation of Na[Al(NH<sub>2</sub>BH<sub>3</sub>)<sub>4</sub>] in the reaction given in Equation (3). Variable-temperature XRPD studies made on **s2** from room temperature to 76 °C at a rate of 1 °C min<sup>-1</sup> have revealed the formation of Na[Al(NH<sub>2</sub>BH<sub>3</sub>)<sub>4</sub>], accompanied by the disappearance of the crystalline precursors (Figure S2 in the Supporting Information). The XRPD patterns collected on **s2** at 76 °C show that Na[Al(NH<sub>2</sub>BH<sub>3</sub>)<sub>4</sub>] gradually decomposes during 1 h with

the formation of NaBH<sub>4</sub> and amorphous product(s) (Figure S2 in the Supporting Information). The same behavior was described by Ohnuki et al.<sup>[26]</sup> However, in their work, numerous peaks were not well resolved, probably, due to a negligible amount of the then-unknown Na[Al(NH<sub>2</sub>BH<sub>3</sub>)<sub>4</sub>] and the limitations of the laboratory XRPD. Indeed, the formation of Na[Al(NH<sub>2</sub>BH<sub>3</sub>)<sub>4</sub>] with high yields requires a long-time milling that was not done earlier. Moreover, the stoichiometry of the starting mixture studied previously was 1:1<sup>[26]</sup> but not 1:4, hence, significantly decreasing the yield. Thus, Na[Al(NH<sub>2</sub>BH<sub>3</sub>)<sub>4</sub>] can be readily obtained by gentle heating of the NaAlH<sub>4</sub>-4 AB composite at about 80 °C. However, the resulting Na[Al(NH<sub>2</sub>BH<sub>3</sub>)<sub>4</sub>] starts to decompose extensively upon keeping it for longer at this temperature. Therefore, this synthetic approach seems to be less attractive and a more reliable alternative synthesis should be suggested. With this in mind, we have directed our attention to long-time ball milling of the NaAlH<sub>4</sub>-4 AB composite at room temperature. Indeed, as a result we have obtained the mixture **s3**, containing about 90 wt% of Na[Al(NH<sub>2</sub>BH<sub>3</sub>)<sub>4</sub>] (Table 1, Figure S3 in the Supporting Information).

We have also attempted to characterize the corresponding Li-containing system,<sup>[23,25,26]</sup> by milling the LiAlH<sub>4</sub>-4 AB composite by using the same experimental conditions as for the Na-containing mixture. However, the reaction has appeared to be extremely violent. In particular, after a few seconds of milling the pressure exceeded twice the calculated value, coming close to the limit of the reaction vial, and as a result, the milling was automatically stopped. Characterization of the resulting sample by PXRD revealed metallic Al and LiBH<sub>4</sub> along with other unidentified phases present as weak peaks (Figure S4 in the Supporting Information). This indicates that the LiAlH<sub>4</sub>-4 AB mixture reacts highly exothermically, and the ball milling is not an appropriate synthesis route.

The formation of borohydrides upon decomposition of Na[Al(NH<sub>2</sub>BH<sub>3</sub>)<sub>4</sub>] of the LiAlH<sub>4</sub>-4 AB composite, also recently found in the reaction products from MH<sub>n</sub>-AB<sup>[23]</sup> and MAIH<sub>4</sub>-AB (M = Li, Na)<sup>[26]</sup> composites, is remarkable. The origin of the BH<sub>4</sub><sup>-</sup> ion in the systems with AB was explained<sup>[27]</sup> by the exchange reaction between its ionic dimer, diammoniate of diborane (DADB) [(NH<sub>3</sub>)<sub>2</sub>BH<sub>2</sub>BH<sub>4</sub>]<sup>[29]</sup> and the alkali-metal alanate salts. This mechanism is not suitable in our case, because NaBH<sub>4</sub> is one of the decomposition products of Na[Al(NH<sub>2</sub>BH<sub>3</sub>)<sub>4</sub>]. Characteristic peaks of NaBH<sub>4</sub> appear immediately after the decomposition of Na[Al(NH<sub>2</sub>BH<sub>3</sub>)<sub>4</sub>]. It should be noted, that the unreacted AB does not participate in this process, because it still remains in the mixture some time after the decomposition of Na[Al(NH<sub>2</sub>BH<sub>3</sub>)<sub>4</sub>] and the appearance of the NaBH<sub>4</sub> peaks (Figure S2 in the Supporting Information). Thus, our work shows that the formation of borohydrides is not an intrinsic property of AB but of the amidoboranes.

### Crystal structure

The crystal structure of Na[Al(NH<sub>2</sub>BH<sub>3</sub>)<sub>4</sub>] was solved in the triclinic space group *P* $\bar{1}$ . The experimental coordinates and those optimized by DFT methods are listed in Table S1 in the Sup-

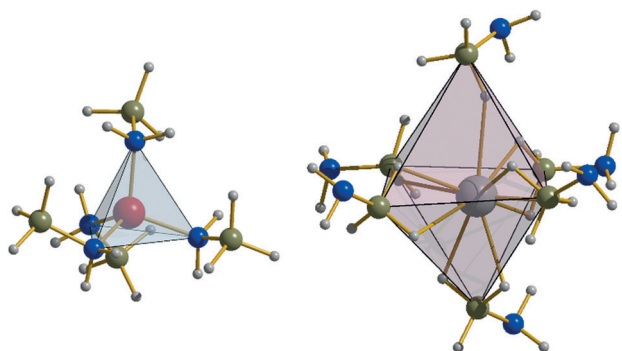


**Figure 2.** Ball and stick plots of the tetrahedral  $[\text{Al}(\text{NH}_2\text{BH}_3)_4]^-$  (left) and the octahedral  $[\text{Na}(\text{NH}_2\text{BH}_3)_6]^{3-}$  (right) fragments. Color code: N = blue, B = olive, H = gray, Al = red, Na = dark gray.

porting Information. Solution of triclinic structures from powder diffraction data is generally difficult, and this is the second amidoborane with a triclinic crystal system, after the mixed-metal complex  $\text{Na}[\text{Li}(\text{NH}_2\text{BH}_3)_2]$ .<sup>[19]</sup> The central  $\text{Al}^{3+}$  atom has a tetrahedral environment formed by four nitrogen atoms from four  $\text{NH}_2\text{BH}_3^-$  ions (Figure 2). Thus, the tetrahedrally configured  $[\text{Al}(\text{NH}_2\text{BH}_3)_4]^-$  ion is a new member of  $\text{Al}^{3+}$  complex hydrides with a tetrahedral coordination, after alanates  $[\text{AlH}_4]^-$ , complex amides  $[\text{Al}(\text{NH}_2)_4]^-$ , and complex borohydrides  $[\text{Al}(\text{BH}_4)_4]^-$ . The  $\text{Na}^+$  atoms are octahedrally coordinated by six  $\text{BH}_3$  groups arising from six  $\text{NH}_2\text{BH}_3^-$  ions (Figure 2), similar to  $\text{Na}^+$  in  $\text{Na}_2[\text{Mg}(\text{NH}_2\text{BH}_3)_4]$ .<sup>[20]</sup> Thus, all  $\text{NH}_2\text{BH}_3^-$  ions exhibit a bridging coordination mode linking  $\text{Al}^{3+}$  and  $\text{Na}^+$  ions with the formation of a 3D polymer structure (Figure 3).

The Al–N bond lengths range from 1.840(9) to 1.929(8) Å and are close to 1.90 Å found in the DFT-optimized experimental model of  $\text{Na}[\text{Al}(\text{NH}_2\text{BH}_3)_4]$ , which, in turn, is slightly longer than 1.85 Å, as observed in  $\text{Na}[\text{Al}(\text{NH}_2)_4]$ .<sup>[30]</sup> The Na...B distances are 2.92(1)–3.55(2) and 2.90–3.64 Å, as evidenced from the PXRD experiments and DFT calculations, respectively. These values are in line with Na...B distances of 2.90–3.63 Å found in  $\text{Na}_2[\text{Mg}(\text{NH}_2\text{BH}_3)_4]$ .<sup>[20]</sup> Remarkably, the dihydrogen N–H<sup>σ+</sup>...H<sup>σ-</sup>–B bonds in  $\text{Na}[\text{Al}(\text{NH}_2\text{BH}_3)_4]$  (1.96(1)–2.28(1) Å from PXRD and 1.92–2.34 Å from DFT calculations) are close to the shortest dihydrogen bonds (1.91(5) Å) in pristine AB,<sup>[27]</sup> and significantly shorter compared to all known MABs (Table S2 in the Supporting Information).<sup>[11–19]</sup>

#### Fourier transform infrared (FTIR) spectroscopy

In order to characterize changes induced by ball milling, FTIR measurements on the mixtures **s2** and **s3** as well as on AB were conducted. The IR spectra of **s2** and **s3** exhibit characteristic bands for the B–H ( $\tilde{\nu}=1100\text{--}1150$  and  $2340\text{--}2420\text{ cm}^{-1}$ ), N–H ( $\tilde{\nu}=1500\text{--}1650$  and  $3200\text{--}3430\text{ cm}^{-1}$ ), and B–N ( $\tilde{\nu}=780\text{ cm}^{-1}$ ) vibration modes similar to those for AB (Figure 4).<sup>[31]</sup> Although the IR spectrum of mixture **s2** shows no significant changes compared to those of the pristine AB and  $\text{NaAlH}_4$ , the spectrum of mixture **s3** contains new bands at  $\tilde{\nu}=630\text{--}673\text{ cm}^{-1}$  assigned to the Al–N vibrational modes (similar to

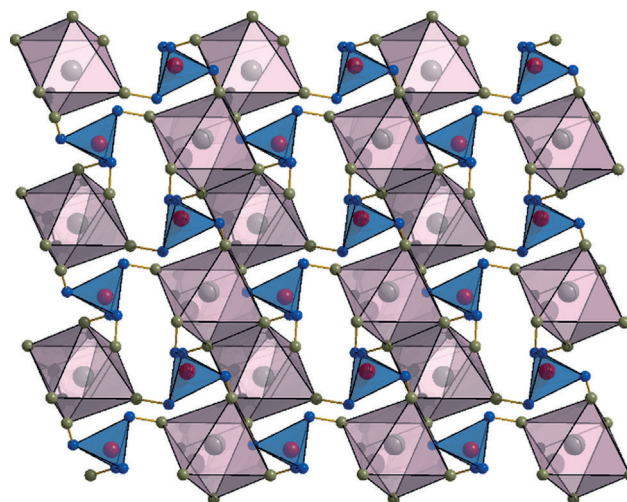
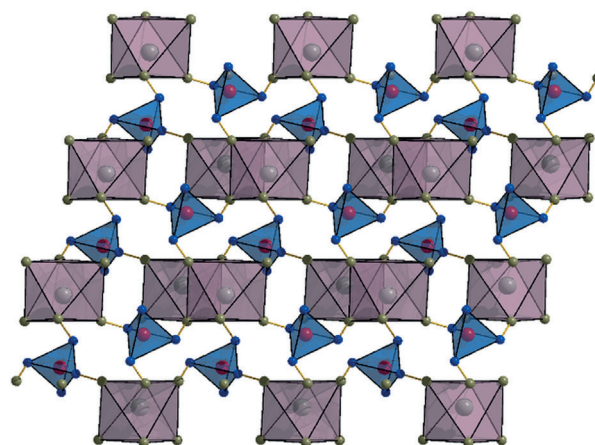
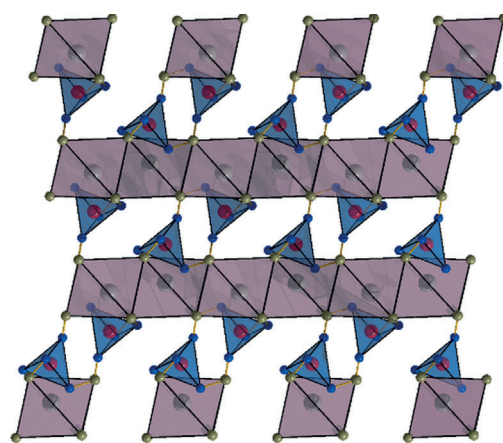


**Figure 3.** Crystal packing of Al and Na coordination polyhedra in the structure of  $\text{Na}[\text{Al}(\text{NH}_2\text{BH}_3)_4]$  along the *a* (top), *b* (middle), and *c* (bottom) axis. Color code: N = blue, B = olive, Al = red, Na = dark gray. Hydrogen atoms are omitted for clarity.

$\text{Na}[\text{Al}(\text{NH}_2)_4]$  and aluminum nitride (AlN)).<sup>[30,32]</sup> Calculated values for the selected vibrational modes in  $\text{Na}[\text{Al}(\text{NH}_2\text{BH}_3)_4]$  are given in Figure S5 in the Supporting Information.

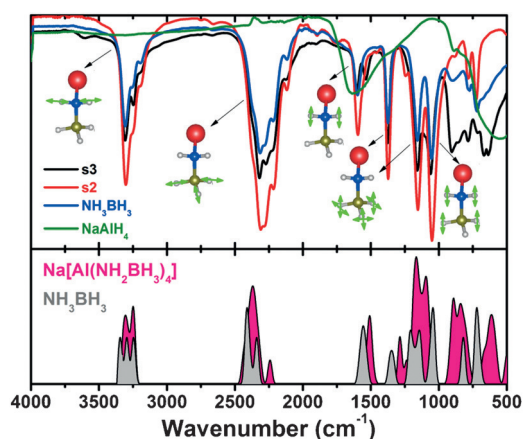


**Figure 4.** FTIR spectra of the mixtures **s2** and **s3** (top). The spectra of  $\text{NH}_3\text{BH}_3$  and  $\text{NaAlH}_4$  are given for comparison. The bottom panel shows the phonon spectra of  $\text{Na}[\text{Al}(\text{NH}_2\text{BH}_3)_4]$  and  $\text{NH}_3\text{BH}_3$ .

### Temperature-programmed photographic analysis

As mentioned in the Introduction, one of the disadvantages of the practical application of AB for hydrogen storage arises from its spectacular foaming leading to a dramatic volume expansion during its thermolysis. With this in mind, we have applied the temperature-programmed photographic analysis to visually observe volume expansion of the mixtures **s2** and **s3** during thermal decomposition from room temperature to 275 °C. The mixture **s2** showed a drastic volume expansion upon heating starting from about 70 °C and increasing up to approximately 110 °C (Figure 5). Under the applied experimental conditions with a heating rate of 5 °C min<sup>-1</sup>, this observation can be explained by the decomposition of the unreacted AB, as its decomposition temperature is at about 107 °C.<sup>[11,33]</sup> Indeed, at around 110 °C the foaming reaches its maximum. The volume of mixture **s3** remained constant under the same experimental conditions (Figure 5), showing a remarkable difference between the starting composite  $\text{NaAlH}_4$ -4AB and the reaction product  $\text{Na}[\text{Al}(\text{NH}_2\text{BH}_3)_4]$ . On the other hand, the foaming of the unreacted AB can be decreased by keeping the

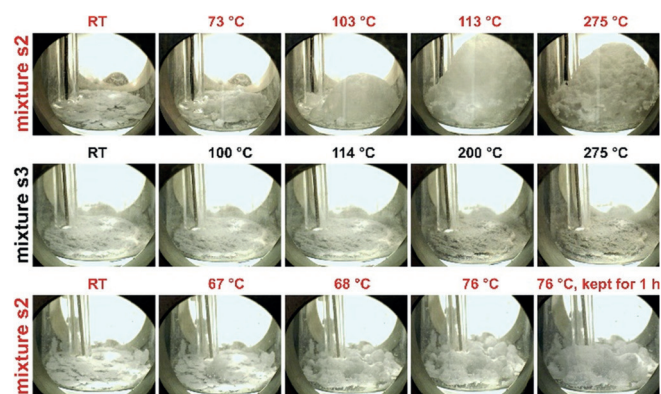


**Figure 5.** Temperature-programmed photographic analysis of the mixtures **s2** and **s3** with a heating rate of 5 °C min<sup>-1</sup>. The foaming during the AB decomposition (top) is not observed for  $\text{Na}[\text{Al}(\text{NH}_2\text{BH}_3)_4]$  (middle), and is suppressed for mixture **s2** by annealing at 76 °C (bottom).

temperature below the decomposition of AB, that is, at 76 °C, where  $\text{Na}[\text{Al}(\text{NH}_2\text{BH}_3)_4]$  is forming from **s2** over about one hour. This is yet another evidence of the formation of  $\text{Na}[\text{Al}(\text{NH}_2\text{BH}_3)_4]$  at temperatures below the decomposition of AB.

### Thermal analysis and mass spectrometry

A simultaneous thermogravimetric analysis–differential scanning calorimetry–mass spectrometry (TGA–DSC–MS) experiment has been conducted for mixture **s2** aiming to characterize the hydrogen release through the formation of  $\text{Na}[\text{Al}(\text{NH}_2\text{BH}_3)_4]$ , and for mixture **s3** aiming to observe the decomposition properties of  $\text{Na}[\text{Al}(\text{NH}_2\text{BH}_3)_4]$ . Thermal decomposition of both samples is described mainly by two resolved steps of weight loss centered at about 120 and 160 °C (Figure 6). The first step in the TGA plot for **s2** is seen as a sharp weight deviation due to the so-called “jet” effect, which is explained by a drastic volume expansion upon heating. This finding is in line with the spectacular foaming, which, in turn, is the result of the decomposition of unreacted AB, as it was observed by the temperature-programmed photographic analysis (Figure 5 and the description above).

Both decomposition steps were found to be exothermic and correspond to hydrogen evolution. An additional exothermic peak was found at about 75 °C for both samples (much less pronounced in the DSC plot of mixture **s3**), and can be explained by the reaction between  $\text{NaAlH}_4$  and AB according to the reaction given in Equation (3). The exothermic peak at 115 °C in the DSC plot of mixture **s2** is the result of the decom-

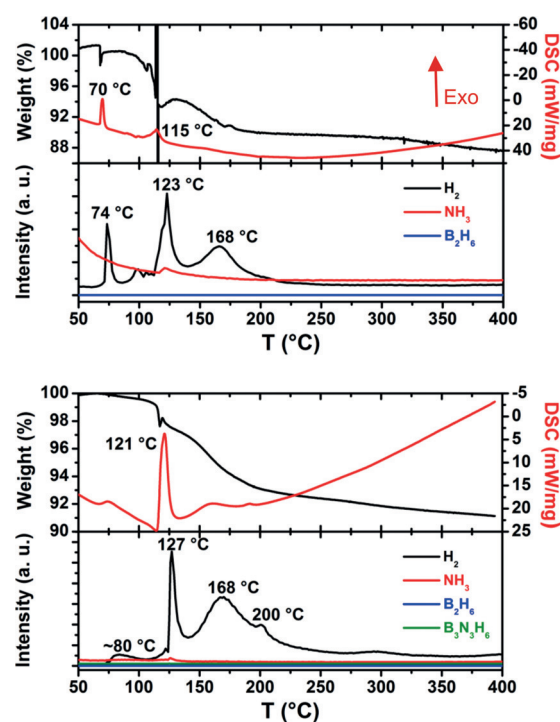


**Figure 6.** TGA–DSC–MS analyses for **s2** (top) and **s3** (bottom) performed under a dynamic argon atmosphere.

position of the unreacted AB, which is in agreement with our PXRD data (Figure S2 in the Supporting Information) and the thermal decomposition pathway of pristine AB.<sup>[10]</sup>

According to the TGA–MS data, neither borazine nor diborane and only traces of ammonia were observed during the decomposition of the mixtures **s2** and **s3** (Figure 6). The total mass loss of approximately 9 wt% for **s3** indicates a partial hydrogen release out of the theoretical 11.9 wt% in Na[Al(NH<sub>2</sub>BH<sub>3</sub>)<sub>4</sub>]. Notably, the formation of Na[Al(NH<sub>2</sub>BH<sub>3</sub>)<sub>4</sub>] from mixture **s2** at a constant temperature of 71 °C results in hydrogen release without detectable impurities of ammonia, diborane, and borazine (Figure S6 in the Supporting Information). The calculated enthalpy of the reaction given in Equation (3) at room temperature was found to be about –25 and –30 kJ mol<sup>–1</sup> (Figure S7 in the Supporting Information), calculated with and without van der Waals interactions, respectively. These results are in agreement with the exothermic events in the DSC data (Figure 6).

### Reaction pathways, volumetric analysis, and reversibility tests

The mixture **s2** heated to 85 °C releases about 3.5 mol of hydrogen per one mole of aluminum (Figure 7). This value is

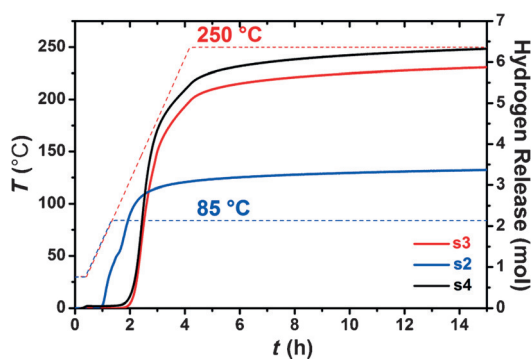


Figure 7. Volumetric desorption curves for the samples **s2**–**s4**.

close to the calculated four moles of hydrogen according to the reaction given in Equation (3), and, together with the diffraction, thermal, and mass spectrometry analyses, proves the formation of Na[Al(NH<sub>2</sub>BH<sub>3</sub>)<sub>4</sub>] during the heating of the NaAlH<sub>4</sub>–4 AB composite.

Volumetric studies of the decomposition of mixture **s3** and of the TiCl<sub>3</sub>-doped but otherwise identical sample **s4** (Table 1) were performed from room temperature up to 250 °C. The decomposition profiles of the samples **s3** and **s4** differ slightly, showing a total hydrogen release of about 6.2 and 6.6 mol per one mole of Na[Al(NH<sub>2</sub>BH<sub>3</sub>)<sub>4</sub>] for samples **s3** and **s4**, respectively (Figure 7).

We have also applied a volumetric technique to study the two decomposition steps centered at about 120 and 160 °C (Figure 6), by fast heating of mixture **s3** to 120 °C, followed by keeping the mixture at this temperature for 60 h, and then by the complete decomposition at 250 °C for about 30 h. Com-

plete separation of these two steps seems impossible due to their partial overlap as evidenced from the TGA–DSC–MS experiments (Figure 6). However, the two decomposition steps are clearly visible on the volumetric curve (Figure S8 in the Supporting Information). The first decomposition step at 120 °C yields approximately 5.3 mol of hydrogen, whereas the total amount of about 8.0 mol is desorbed at 250 °C. These data confirm the prevalent formation of hydrogen: the weight loss of about 9 wt% in the TGA is in agreement with eight mole of hydrogen gas found volumetrically.

The absence of crystalline Al and Na<sub>3</sub>AlH<sub>6</sub> (the decomposition products of NaAlH<sub>4</sub>)<sup>[4]</sup> of the boron nitride (BN), which can be formed during the decomposition of AB,<sup>[10,11]</sup> as well as of AlN, which hypothetically can form through the decomposition of Na[Al(NH<sub>2</sub>BH<sub>3</sub>)<sub>4</sub>] at 250 °C has been shown by XRPD (Figure S9 in the Supporting Information). The only crystalline phase present there is NaBH<sub>4</sub>. However, the FTIR spectrum of the final residue reveals all characteristic bands of NaBH<sub>4</sub> and a number of additional bands suggesting the presence of the Al–N, B–N, B–H, and N–H groups. The latter two bands are similar to those observed upon thermal decomposition of the pristine AB with the formation of polymeric (NH<sub>x</sub>BH<sub>x</sub>)<sub>n</sub> (1 ≤ x ≤ 2) species (Figure S10 in the Supporting Information).<sup>[31,32]</sup> Furthermore, in resemblance to binary amidoboranes M(NH<sub>2</sub>BH<sub>3</sub>)<sub>n</sub> (n = 1, M = Li<sup>+</sup>, Na<sup>+</sup>, K<sup>+</sup>; n = 2, M = Ca<sup>2+</sup>, Mg<sup>2+</sup>)<sup>[15,34–36]</sup> and to the Li<sub>3</sub>AlH<sub>6</sub>–4 AB<sup>[25]</sup> system, we observed the formation of amorphous product(s), most likely, of the hydrogen-poor Al–N–B–H composition(s). Interestingly, recent theoretical calculations of the decomposition mechanism of Al(NH<sub>2</sub>BH<sub>3</sub>)<sub>3</sub> propose the formation of Al(NBH<sub>3</sub>)<sub>3</sub>.<sup>[37]</sup> However, to the best of our knowledge, no experimental evidence of the existence of Al(NH<sub>2</sub>BH<sub>3</sub>)<sub>3</sub> was reported so far. Taking into account all the data on the decomposition pathway of Na[Al(NH<sub>2</sub>BH<sub>3</sub>)<sub>4</sub>] obtained in this work, the following simplified total decomposition reaction can be suggested [Eq. (4)]:



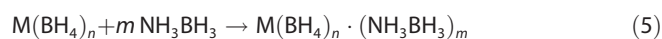
Two regeneration tests were performed for the samples **s3** and **s4** by applying 150 bar of hydrogen: one at 85 °C, to check for a hypothetical transformation back to the starting NaAlH<sub>4</sub>–4 AB composite, and another at 250 °C, to attempt a rehydrogenation of AlN<sub>4</sub>B<sub>3</sub>H<sub>(0-3.6)</sub>. It was found that Na[Al(NH<sub>2</sub>BH<sub>3</sub>)<sub>4</sub>] does not take up hydrogen at temperatures up to 85 °C but instead decomposes slowly (Figures S11a and e in the Supporting Information). Thus, the final uptake was negative for both samples **s3** and **s4**. This behavior is expected, because the reaction given in Equation (3) is slightly exothermic according to the DSC data (Figure 6) and the DFT calculations (Figure S7 in the Supporting Information).

Slow hydrogen absorption was observed at 250 °C for the completely decomposed samples **s3** and **s4** (Figures S11b and f in the Supporting Information). Surprisingly, about 1.7 out of 6.2 mol (≈ 27%) of the released hydrogen have been absorbed by the amorphous residue during approximately 225 h (Figures S11c and g in the Supporting Information). The absorbed amount can be readily released (Figures S11d and h in the

Supporting Information). This reversible absorption can be due to the hydrogen uptake with the formation of the amorphous intermediate(s) observed between the two decomposition steps at 120 and 160 °C (Figure 1). This scenario is likely, because in situ XRPD done at 250 °C and 150 bar of hydrogen did not show any crystalline phases forming upon the rehydrogenation during 26 h of the decomposed sample **s3** (Figure S9 in the Supporting Information). This rehydrogenation can be a result of a continuous hydrogen absorption in the amorphous compound  $\text{AlN}_4\text{B}_3\text{H}_{(0-3.6)}$  to phases with a higher hydrogen content.

## Conclusions

The new  $\text{NaAlH}_4\text{-4AB}$  composite, combining complex and chemical hydrides, releases pure hydrogen and produces the first Al-based amidoborane,  $\text{Na}[\text{Al}(\text{NH}_2\text{BH}_3)_4]$ . The reaction proceeds already at 70 °C or under mechanochemical treatment at room temperature. This is the first example of a reaction where a complex hydride anion is deprotonating AB. Until now only binary metal hydrides were reacted with AB, forming amidoboranes [see the equation given in Equation (2)]. Breaking of the Al–H bonds in the  $\text{AlH}_4^-$  ion is, apparently, easier than the breaking of the B–H bonds in the  $\text{BH}_4^-$  ion as the latter one does not deprotonate AB. Therefore, alkali and alkali-earth metal borohydrides ( $\text{M}=\text{Li}^+$ ,  $\text{Mg}^{2+}$ , and  $\text{Ca}^{2+}$ ) merely form adducts with AB [Eq. (5)].<sup>[38–42]</sup>



The formation of  $\text{Na}[\text{Al}(\text{NH}_2\text{BH}_3)_4]$  by the reaction given in Equation (3) is not reversible at 150 bar of hydrogen, which is in line with the observed exothermic dehydrogenation. Therefore, an RHC based on this reaction [Eq. (3)] cannot be used as a reversible hydrogen store.

$\text{Na}[\text{Al}(\text{NH}_2\text{BH}_3)_4]$  decomposes in two steps with the formation of  $\text{NaBH}_4$ , up to eight equivalents of pure hydrogen and an amorphous product  $\text{AlN}_4\text{B}_3\text{H}_{(0-3.6)}$ . The latter reversibly reabsorbs about 27% of hydrogen. This re-absorption regenerates neither  $\text{NaAlH}_4$  nor  $\text{Na}[\text{Al}(\text{NH}_2\text{BH}_3)_4]$  but occurs between the amorphous product and the intermediate(s) of the dehydrogenation. Further in-depth studies of  $\text{AlN}_4\text{B}_3\text{H}_{(0-3.6)}$ , that is, its chemical structure and an optimization of the rehydrogenation process, are required.

During the recent years, Al-based complex hydrides attract an ever-growing attention as potential hydrogen storage media. Indeed, the reaction given in Equation (3) is possible not only because the Al–H bonds are less stable than the B–H ones, but also due to the strong Lewis acidity of the  $\text{Al}^{3+}$  ion forming the tetraamidoborane complex. The title system opens an avenue to a series of aluminum tetraamidoboranes,  $\text{M}[\text{Al}(\text{NH}_2\text{BH}_3)_4]$ , with improved hydrogen storage properties, such as the hydrogen storage density, the hydrogen purity and reversibility. Our preliminary experiments, not presented in this work, show that the reaction given in Equation (3) easily proceeds in THF solution at room temperature, and these condi-

tions are successfully applied to the reaction in the  $\text{LiAlH}_4\text{-4AB}$  system, uncontrollable in the solid state.

Future works can also exploit the combination of amidoborane and borohydride ligands in the same Al-based compound, tuning their stability through different electron donor–acceptor properties of the ligands. Recent discovery of the  $\text{M}[\text{Al}(\text{BH}_4)_4]$  series<sup>[43]</sup> allows this goal to be achieved in a one-step reaction with  $\text{M}[\text{Al}(\text{NH}_2\text{BH}_3)_4]$ .

## Experimental Section

**Materials and synthesis:** All samples were obtained from commercially available  $\text{LiAlH}_4$ ,  $\text{NaAlH}_4$ ,  $\text{TiCl}_3$ , and  $\text{NH}_3\text{BH}_3$  (95, 93, 99.99, and 98% purity, respectively) purchased from Alfa Aesar, Sigma Aldrich Co, and Katchem. All operations were done in gloveboxes with a high purity argon atmosphere. The starting materials were placed into stainless steel vials and milled in a planetary ball mill Fritsch Pulverisette 7, by using Easy GTM gas pressure and a temperature detection system for monitoring the reaction. The gas release measured during the ball milling for the  $\text{NaAlH}_4\text{-4AB}$  composite is shown in Figure S12 in the Supporting Information. The rotation speed was set to 600 rpm and the ball to the powder mass ratio to 30:1. Synthetic approaches for different samples are listed in Table 1.

**X-ray powder diffraction analysis (XRPD):** Samples were filled into 0.5 mm thin-walled glass capillaries and sealed under an argon atmosphere. Laboratory diffraction data were obtained with a MAR345 diffractometer, rotating anode  $\text{MoK}\alpha$  radiation, and a XENOCs focusing mirror. Sample **s3** was tested for rehydrogenation by using a sapphire-based cell for in situ XRPD.<sup>[44]</sup> The starting powder was kept in a single-crystal sapphire capillary with an outer diameter of 1.09 mm. Decomposition of  $\text{Na}[\text{Al}(\text{NH}_2\text{BH}_3)_4]$  under 5 bar of hydrogen was performed by heating the capillary from room temperature to 250 °C with a heating rate of  $1^\circ\text{Cmin}^{-1}$ . The decomposed sample was heated to 250 °C under 150 bar of hydrogen, whereas powder diffraction data was continuously collected for approximately 26 h.

**Variable-temperature in situ synchrotron X-ray powder diffraction (SRXRPD):** SRXRPD data were collected with a PILATUS@SNBL diffractometer (SNBL, ESRF, Grenoble, France) equipped with a Dectris PILATUS 2M single-photon counting pixel area detector ( $\lambda = 0.823065 \text{ \AA}$ ). Temperature was increased linearly in time by using an Oxford Cryostream 700+ with a heating rate of  $5^\circ\text{Cmin}^{-1}$  from room temperature to 150 °C. Powder patterns were obtained by using raw and integrated data preprocessed by the SNBL Toolbox software and data of the  $\text{LaB}_6$  standard.<sup>[45]</sup>

**Crystal structure determination:** The SRPXRD data for mixture **s1** at 100 °C were indexed in a triclinic crystal lattice and the structure of  $\text{Na}[\text{Al}(\text{NH}_2\text{BH}_3)_4]$  was solved in the  $P\bar{1}$  space group by using the program FOX.<sup>[46]</sup> The ADDSYM procedure did not reveal a higher symmetry. The obtained crystal structure was further optimized by DFT calculations (see below) in order to obtain accurate hydrogen atom positions. The final structure, obtained from the DFT calculations, was refined by using bond distance restraints for the hydrogen atoms by the Rietveld method by using Fullprof (Figure 8).<sup>[47]</sup> The Supporting Information contains the experimental and DFT-optimized crystal structures as CIF files.

**DFT optimization:** The structure of  $\text{Na}[\text{Al}(\text{NH}_2\text{BH}_3)_4]$  was optimized by simulated annealing within the plane wave formulation of the DFT method.<sup>[48]</sup> Electronic configurations of  $1s^1$  for H,  $2s^22p^1$  for B,  $2s^22p^3$  for N,  $2p^63s^1$  for Na, and  $3s^23p^1$  for Al were represented by

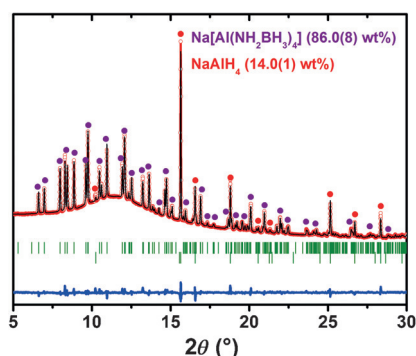


**Figure 8.** Rietveld refinement profile ( $R_{wp} = 12.7\%$ ) for mixture **s1** at  $100\text{ }^\circ\text{C}$  (SNBL/SRF synchrotron,  $\lambda = 0.823065\text{ \AA}$ ).  $\text{Na}[\text{Al}(\text{NH}_2\text{BH}_3)_4]$ : triclinic; space group  $P\bar{1}$ ;  $a = 9.4352(2)$ ,  $b = 7.7198(1)$ ,  $c = 7.6252(1)\text{ \AA}$ ;  $\alpha = 97.211(1)$ ,  $\beta = 109.223(2)$ ,  $\gamma = 89.728(2)^\circ$ ;  $R_F = 5.7\%$ .  $\text{NaAlH}_4$ : tetragonal; space group  $I4_1/a$ ;  $a = 5.0398(1)$ ,  $b = 11.4319(1)\text{ \AA}$ ;  $R_F = 6.7\%$ .

projected augmented wave potentials.<sup>[49]</sup> The gradient-corrected (GGA) functional<sup>[50]</sup> and the correction for weak dispersive interaction were applied.<sup>[51]</sup> The initial structure from the Rietveld refinement was optimized with respect to the internal atomic positions and the unit cell shape. This optimized structure was heated to  $T = 400\text{ K}$  with a rate of  $100\text{ Kps}^{-1}$  and cooled down to  $T = 0\text{ K}$  with a rate of  $20\text{ Kps}^{-1}$ . No constraints were imposed on the internal atomic positions and the unit cell parameters were kept fixed. A Nose–Hoover thermostat<sup>[53,54]</sup> was applied for this procedure, and the time step for integration of equations of motion was  $0.6\text{ fs}$ . Six independent structures with the lowest energy from the temperature range below  $50\text{ K}$  were optimized with respect to internal atomic positions with a conjugated gradient method; then the symmetry was determined to be  $P\bar{1}$  for five structures with the lowest ground state energy. For these structures the symmetry was imposed and the unit cell shape, together with the atomic positions, was re-optimized. Within the accuracy of the GGA calculations all five structures were identical with the following lattice parameters at the ground state:  $a = 9.435$ ,  $b = 7.719$ ,  $c = 7.625\text{ \AA}$ ;  $\alpha = 97.213$ ,  $\beta = 109.219$ ,  $\gamma = 89.725^\circ$ . The total energy of the optimized structure was  $0.03\text{ eV}$  per formula unit lower than that for the initial guess. The normal mode analysis was performed with finite displacement method for the  $\Gamma$  point; atoms were displaced by  $\pm 0.25\text{ \AA}$  along each Cartesian direction. All modes are real positive.

In order to assess the enthalpy of the reaction given in Equation (3), the ground state and the vibrational properties were calculated for AB and  $\text{NaAlH}_4$ , based on their crystal structures.<sup>[54,55]</sup> For all systems two independent calculations were done with and without corrections for weak dispersive interactions. The enthalpy was calculated within an harmonic approximation.<sup>[56]</sup> Thus, it consists of the electronic ground state energy and the contribution from the vibrational degrees of freedom.

For the phonon calculations the dynamical matrix was constructed from the forces excerpted on atoms upon displacements. The dynamical matrix was diagonalized and the normal mode frequencies and polarization vectors were extracted. The enthalpy of the reaction given in Equation (3),  $H(T) = E_0 + H_{\text{vibra}}(T)$ , was calculated within the harmonic approximation as a sum of vibrational  $H_{\text{vibra}}(T) = \sum \frac{1}{2} \hbar \pi_i + \sum \hbar \pi_i \left( \exp\left(\frac{\hbar \pi_i}{kT}\right) - 1 \right)^{-1}$  and electronic contributions at the ground state  $E_0$  for each reactant and products ( $\omega_i$  is the normal mode frequency at  $T = 0\text{ K}$ ,  $k$  is the Boltzmann constant). For the hydrogen in the gas-phase terms related to rotation-

al, translational, and  $pV$  are added as  $(7/2)kT$ . The ground state energy normal modes were calculated for two independent cases: with and without weak van der Waals forces. For AB the later interactions are important. The lattice parameters calculated for the ground state are given in Table S3 in the Supporting Information.

**Fourier transform infrared spectroscopy (FTIR):** Infrared spectra were recorded with a NICOLET 380 FTIR spectrometer from Thermo Electron Corporation. Samples were exposed to air for about  $15\text{ s}$  when transferring from the sample vial to the instrument. In order to determine the decomposition products of mixture **s3**, the same measurements were performed after its heating in a Schlenk tube under argon atmosphere at  $250\text{ }^\circ\text{C}$  for  $3\text{ h}$ .

**Thermal analysis and mass spectrometry:** Thermogravimetric analysis and differential scanning calorimetry were measured by using a Perkin–Elmer STA 6000 apparatus simultaneously with mass spectrometry analysis of the residual gas with the use of a Hiden Analytical HPR-20 QMS sampling system. The samples ( $\approx 2\text{ mg}$ ) were loaded into an  $\text{Al}_2\text{O}_3$  crucible and heated from room temperature to  $400\text{ }^\circ\text{C}$  ( $5\text{ }^\circ\text{Cmin}^{-1}$ ) in an argon flow of  $20\text{ mLmin}^{-1}$ . The released gases were analyzed for hydrogen, ammonia, diborane, and borazine.

**Temperature-programmed photographic analysis (TPPA):** Aliquots of samples **s2** and **s3** ( $10\text{ mg}$ ) were sealed under argon in a glass tube placed in a home-built aluminum heating block as described recently.<sup>[57]</sup> Samples were heated from room temperature to  $300\text{ }^\circ\text{C}$  ( $\Delta T/\Delta t = 5\text{ }^\circ\text{Cmin}^{-1}$ ), sample **s2** was also heated from room temperature to  $76\text{ }^\circ\text{C}$  ( $\Delta T/\Delta t = 3\text{ }^\circ\text{Cmin}^{-1}$ ) and kept at this temperature for  $1\text{ h}$ . Photos of the samples were collected every five seconds.

**Volumetric analysis and reversibility tests:** Volumetric analysis was performed by using a Hiden Isochema IMI-SHP analyzer. Aliquots of samples **s2–s4** ( $40\text{–}50\text{ mg}$ ) were heated from  $30$  to  $85$  and to  $250\text{ }^\circ\text{C}$  ( $1\text{ }^\circ\text{Cmin}^{-1}$ ,  $p(\text{H}_2) = 5\text{ bar}$ ). Subsequently, rehydrogenation was performed at  $p(\text{H}_2) = 150\text{ bar}$  by heating sample **s2** to  $85\text{ }^\circ\text{C}$ , and samples **s3** and **s4** to  $250\text{ }^\circ\text{C}$  ( $0.1\text{ }^\circ\text{Cmin}^{-1}$ ). Gas release was calculated from the calibrated volumes of the system, excluding the volume of the glass wool ( $2.06\text{ gcm}^{-3}$ ). The final uptake was calculated from the difference between the average start uptake at  $30\text{ }^\circ\text{C}$  (equal to the temperature of the manifold) and the decomposition uptake after cooling to the same temperature, in order to decrease uncertainties of calibrations. Usually, the uptake calculated by the manifold's IMI software at  $250\text{ }^\circ\text{C}$  is about  $3\%$  lower ( $\approx 0.2\text{ mol}$ ) than at  $30\text{ }^\circ\text{C}$ .

## Acknowledgements

This work was supported by the Académie Universitaire Louvain (AUL, Belgium) under Grant ADi/DB/1058.2011 and the FNRS (CC 1.5169.12, PDR T.0169.13, EQP U.N038.13). D.A.S. thanks the WBI (Belgium) for the post-doctoral position. We thank the ESRF for the beamtime allocation at the SNBL. Z.Ł. acknowledges CPU allocation at PLGrid Infrastructure and support by a grant from Switzerland through the Swiss Contribution to the enlarged European Union.

**Keywords:** boranes · crystal engineering · hydrides · hydrogen storage · sodium alanate

[1] L. E. Klebanoff, J. O. Keller, *Int. J. Hydrogen Energy* **2013**, *38*, 4533–4576.

- [2] S. Orimo, Y. Nakamori, J. R. Eliseo, A. Züttel, C. M. Jensen, *Chem. Rev.* **2007**, *107*, 4111–4132.
- [3] M. B. Ley, L. H. Jepsen, Y.-S. Lee, Y. W. Cho, J. B. Colbe, M. Dornheim, M. Rokhi, J. O. Jensen, M. Sloth, Y. Filinchuk, J. E. Jørgensen, F. Besenbacher, T. R. Jensen, *Mater. Today* **2014**, *17*, 122–128.
- [4] B. Bogdanovich, M. Schwickardi, *J. Alloys Compd.* **1997**, *253–254*, 1–9.
- [5] J. J. Vajo, S. L. Skeith, F. Meriens, *J. Phys. Chem. B* **2005**, *109*, 3719–3722.
- [6] U. Bösenberg, S. Doppiu, L. Mosegaard, G. Barkhordarian, N. Eigen, A. Borgshulte, T. R. Jensen, Y. Cerenius, O. Gutfleisch, T. Klassen, M. Dornheim, R. Bormann, *Acta Mater.* **2007**, *55*, 3951–3958.
- [7] Y. S. Chua, P. Chen, G. Wu, Z. Xiong, *Chem. Commun.* **2011**, *47*, 5116–5129.
- [8] L. H. Jepsen, M. B. Ley, Y.-S. Lee, Y. W. Cho, M. Dornheim, J. O. Jensen, Y. Filinchuk, J. E. Jørgensen, F. Besenbacher, T. R. Jensen, *Mater. Today* **2014**, *17*, 129–135.
- [9] A. Staubitz, A. P. M. Robertson, I. Manners, *Chem. Rev.* **2010**, *110*, 4079–4124.
- [10] G. Wolf, J. Baumann, F. Baitalow, F. P. Hoffmann, *Thermochim. Acta* **2000**, *343*, 19–25.
- [11] F. Baitalow, J. Baumann, G. Wolf, K. Jaenicke-Rößler, G. Leiter, *Thermochim. Acta* **2002**, *391*, 159–168.
- [12] Z. Xiong, C. K. Yong, G. Wu, P. Chen, W. Shaw, A. Karkamkar, T. Autrey, M. O. Jones, S. I. Johnson, P. P. Edwards, W. I. F. David, *Nat. Mater.* **2008**, *7*, 138–141.
- [13] H. V. K. Diyabalanage, T. Nakagawa, R. P. Shrestha, T. A. Semelsberger, B. L. Davis, B. L. Scott, A. K. Burell, W. I. F. David, K. R. Ryan, M. O. Jones, P. P. Edwards, *J. Am. Chem. Soc.* **2010**, *132*, 11836–11837.
- [14] H. V. K. Diyabalanage, R. P. Shrestha, T. A. Semelsberger, B. L. Scott, M. E. Bowden, B. L. Davis, A. K. Burelli, *Angew. Chem. Int. Ed.* **2007**, *46*, 8995–8997; *Angew. Chem.* **2007**, *119*, 9153–9155.
- [15] H. Wu, W. Zhou, T. Yildirim, *J. Am. Chem. Soc.* **2008**, *130*, 14834–14839.
- [16] J. Luo, X. Kang, P. Wang, *Energy Environ. Sci.* **2013**, *6*, 1018–1025.
- [17] Q. Zhang, C. Tang, C. Fang, F. Fang, D. Sun, L. Ouyang, M. Zhu, *J. Phys. Chem. C* **2010**, *114*, 1709–1714.
- [18] R. V. Genova, K. J. Fijalkowski, A. Budzianowski, W. Grochala, *J. Alloys Compd.* **2010**, *499*, 144–148.
- [19] K. J. Fijalkowski, R. V. Genova, Y. Filinchuk, A. Budzianowski, M. Derzci, T. Jaroń, P. J. Leszczynski, W. Grochala, *Dalton Trans.* **2011**, *40*, 4407–4413.
- [20] H. Wu, W. Zhou, F. E. Pinkerton, M. S. Meyer, Q. Yao, S. Gadipelli, T. Yildirim, J. J. Rush, *Chem. Commun.* **2011**, *47*, 4102–4204.
- [21] Y. S. Chua, W. Li, G. Wu, Z. Xiong, P. Chen, *Chem. Mater.* **2012**, *24*, 3574–3581.
- [22] C. Wu, G. Wu, Z. Xiong, X. Han, H. Chu, T. He, P. Chen, *Chem. Mater.* **2010**, *22*, 3–5.
- [23] Y. Nakagawa, S. Isobe, Y. Ikarashi, S. Ohnuki, *J. Mater. Chem. A* **2014**, *2*, 3926–3931.
- [24] Y. Zhang, K. Shimoda, H. Miyaoka, T. Ichikawa, Y. Kojima, *Int. J. Hydrogen Energy* **2010**, *35*, 12405–12409.
- [25] G. Xia, Y. Tan, X. Chen, Z. Guo, H. Liu, X. Yu, *J. Mater. Chem. A* **2013**, *1*, 1810–1820.
- [26] Y. Nakagawa, Y. Ikarashi, S. Isobe, S. Hino, S. Ohnuki, *RSC Adv.* **2014**, *4*, 20626–20631.
- [27] M. E. Bowden, G. J. Gainsford, W. T. Robinson, *Aust. J. Chem.* **2007**, *60*, 149–153.
- [28] B. C. Hauback, H. W. Brinks, C. M. Jensen, K. Murphy, A. J. Maeland, *J. Alloys Compd.* **2003**, *358*, 142–145.
- [29] A. C. Stowe, W. J. Shaw, J. C. Linehan, B. Schmid, T. Autrey, *Phys. Chem. Chem. Phys.* **2007**, *9*, 1831–1836.
- [30] H. D. Lutz, N. Lange, *Z. Anorg. Allg. Chem.* **1992**, *613*, 83–87.
- [31] J. Baumann, F. Baitalow, G. Wolf, *Thermochim. Acta* **2005**, *430*, 9–14.
- [32] X. Chen, K. E. Gonsalves, *J. Mater. Res.* **1997**, *12*, 1274–1286.
- [33] M. G. Hu, R. A. Geanangel, W. W. Wendlandt, *Thermochim. Acta* **1978**, *23*, 249–255.
- [34] K. Shimoda, K. Doi, T. Nakagawa, Y. Zhang, H. Miyoaka, T. Ishikawa, M. Tansho, T. Shimizu, A. K. Burell, Y. Kojima, *J. Phys. Chem. C* **2012**, *116*, 5957–5964.
- [35] K. Shimoda, Y. Zhang, T. Ishikawa, Y. Kojima, *J. Mater. Chem.* **2011**, *21*, 2609–2615.
- [36] F. Leardini, J. R. Ares, J. Bodega, M. J. Valero-Pedraza, M. A. Bañares, J. F. Fernández, C. Sánchez, *J. Phys. Chem. C* **2012**, *116*, 24430–24435.
- [37] K. Wang, V. Arcisauskaitė, J.-S. Jiao, J.-G. Zhang, T.-L. Zhang, Z.-N. Zhou, *RSC Adv.* **2014**, *4*, 14624–14632.
- [38] L. H. Jepsen, J. Skibsted, T. R. Jensen, *J. Alloys Compd.* **2013**, *580*, S287–S291.
- [39] J. Luo, H. Wu, W. Zhou, X. Kang, Z. Fang, P. Wang, *Int. J. Hydrogen Energy* **2012**, *37*, 10750–10757.
- [40] H. Wu, W. Zhou, F. E. Pinkerton, M. S. Meyer, G. Srinivas, T. Yildirim, T. J. Udovic, J. J. Rush, *J. Mater. Chem.* **2010**, *20*, 6550–6556.
- [41] X. Chen, F. Yuan, Q. Gu, X. Yu, *Dalton Trans.* **2013**, *42*, 14365–14368.
- [42] L. H. Jepsen, V. Ban, K. T. Møller, Y.-S. Lee, Y. W. Cho, F. Besenbacher, Y. Filinchuk, J. Skibsted, T. R. Jensen, *J. Phys. Chem. C* **2014**, *118*, 12141–12153.
- [43] I. Dovgaliuk, V. Ban, Y. Sadikin, R. Cerný, L. Aranda, N. Casati, M. Devillers, Y. Filinchuk, *J. Phys. Chem. C* **2014**, *118*, 145–153.
- [44] T. R. Jensen, T. K. Nielsen, Y. Filinchuk, J.-E. Jørgensen, Y. Cerenius, E. M. Gray, C. J. Webb, *J. Appl. Crystallogr.* **2010**, *43*, 1456–1463.
- [45] SNBL ToolBox, V. Dyadkin, Swiss–Norwegian Beam Lines at the ESRF, Grenoble (France), Release **2014**–2.
- [46] V. Favre-Nicolin, R. Černý, *J. Appl. Crystallogr.* **2002**, *35*, 734–743.
- [47] J. Rodríguez-Carvajal, *J. Physica B.* **1993**, *192*, 55–69.
- [48] G. Kresse, J. Furthmüller, *Phys Rev B* **1996**, *54*, 11169–11186.
- [49] P. E. Blöchl, *Phys. Rev. B* **1994**, *50*, 17953–17989.
- [50] J. P. Perdew, K. Burke, M. Ernzerhof, *Phys. Rev. Lett.* **1996**, *77*, 3865–3868.
- [51] S. Grimme, *J. Comp. Chem.* **2006**, *27*, 1787–1799.
- [52] S. Nosé, *J. Chem. Phys.* **1984**, *81*, 511–519.
- [53] W. G. Hoover, *Phys. Rev. A* **1985**, *31*, 1695–1697.
- [54] W. T. Klooster, T. F. Koetzle, P. E. M. Siegbahn, T. B. Richardson, R. H. Crabtree, *J. Am. Chem. Soc.* **1999**, *121*, 6337–6343.
- [55] K. J. Gross, S. Guthrie, S. Takara, G. Thomas, *J. Alloys Compd.* **2000**, *297*, 270–281.
- [56] M. Born, K. Huang, *Dynamical Theory of Crystal Lattices*, Oxford University Press, Oxford, **1954**.
- [57] M. Paskevicius, M. B. Ley, D. A. Shepard, T. R. Jensen, C. E. Buckley, *Phys. Chem. Chem. Phys.* **2013**, *15*, 19774–19789.

Received: April 2, 2015

Published online on August 26, 2015